INSTITUTE OF PHYSICS PUBLISHING PHYSICS IN MEDICINE AND BIOLOGY

Phys. Med. Biol. **50** (2005) 4429–4444 doi:10.1088/0031-9155/50/18/012

Ellipsoidal electrogastrographic forward modelling

Andrei Irimia and L Alan Bradshaw

Living State Physics Laboratories, Department of Physics and Astronomy, Vanderbilt University, Nashville, TN 37235-1807, USA

Received 25 May 2005, in final form 6 July 2005
Published 7 September 2005
Online at stacks.iop.org/PMB/50/4429

Abstract

The theoretical and computational study of the electromagnetic forward and inverse problems in ellipsoidal geometry is important in electrogastrography because the geometry of the human stomach can be well approximated using this idealized body. Moreover, the anisotropies inherent to this organ can be highlighted by the characteristics of the electric potential associated with current dipoles in an ellipsoid. In this paper, we present a forward simulation for the stomach using an analytic expression of the gastric electric potential that employs a truncated expansion of ellipsoidal harmonics; we then demonstrate that an activation front of dipoles propagating along the body of an ellipsoid can simulate gastric electrical activity. In addition to the usefulness of our model, we also discuss its limitations and accuracy.

(Some figures in this article are in colour only in the electronic version)

1. Introduction

The scientific area of electro- and magnetogastrography (EGG and MGG) has become increasingly important in recent years to both clinicians and biophysicists due to the ever-increasing body of evidence indicating that noninvasive methods of gastrointestinal (GI) disease diagnosis are within sight. Physiologically, electric fields in the human gut are produced by the exchange of ions between cells in the gastric smooth muscle. The movement of these ions creates electric currents that generate magnetic fields; although of the order of pT, these fields can be detected noninvasively using Superconducting QUantum Interference Device (SQUID) magnetometers. SQUIDs are devices equipped with Josephson junctions that are capable of sustaining supercurrents below the critical temperature of the metal of which these junctions are made. Due to their design and certain properties of superconductors, SQUIDs have the ability to measure extremely small changes in magnetic flux, which makes them unrivaled among magnetomers in terms of sensitivity.

SQUIDs have been used to measure the weak fields of various human organs, including the brain (electro- and magnetoencephalography), heart (electro- and magnetocardiography (Jenks *et al* 1997)) and the stomach (EGG and MGG). With over 60 million patients receiving treatment for GI diseases every year just in the US, the importance of early diagnosis and

treatment of gut diseases cannot be overstated. The use of SQUID magnetometry for the clinical study of gastric pathology was pioneered in the early 1990s in the Living State Physics Laboratories at Vanderbilt University. Since then, it has been shown that SQUIDs are capable of recording abnormal magnetic field patterns associated with various important gut diseases, such as ischemia, gastroparesis (Rothstein *et al* 1993) and venous thrombosis (Allos *et al* 1997). This is particularly important in light of the fact that the fatality rate for acute mesenteric ischemia is over 50% (Everhart 1994), a figure that could possibly be lowered dramatically if efficient, noninvasive diagnosis tools became widely available.

In the normal stomach, gastric electrical activity (GEA) manifests itself as an electric wave that propagates across the organ with a periodicity of 3 cycles per minute (cpm) (Sharkawi *et al* 1978, Turnbull *et al* 1999). GEA propagation starts in the upper portion of the gastric corpus in a region of the organ that behaves like an electrical syncytium; it then advances along the corpus in the direction of the pylorus with increasing velocity, whereafter it resets again to the upper corpus and the cycle repeats (Jiménez *et al* 1999, Lin *et al* 2000). GEA is mediated by the presence of the cells of Cajal (Sanders 1996, Serio *et al* 1991), which are shown to be at the origin of the propagation phenomenon. In an important study conducted at Vanderbilt University (Bradshaw *et al* 1997), it was demonstrated that the normal magnetic and electric field propagation patterns of the stomach are disrupted in the event of ischemia, which immediately drew attention to the possible use of SQUIDs as diagnosis tools for the detection of this and other diseases (Mintchev *et al* 1997).

To study GEA, one must become aware of how electric sources move along the body of the stomach during propagation. To identify the locations and orientations of these sources based on SQUID recordings of magnetic fields, one must solve the biomagnetic inverse problem. The related problem of computing the electric potential, electric field or magnetic field from known current distributions is known as the forward problem. Numerous theoretical and computational models attempting to capture the characteristics of GEA have appeared in the literature (Irimia and Bradshaw 2003, Mirizzi and Scafoglieri 1983, Nelsen and Becker 1968, Publicover and Sanders 1989, Rashev *et al* 2000), all falling into one of two broad categories, i.e. idealized or realistic. Idealized models have the advantage of simplicity since they allow both the forward and inverse problems to be studied with relative ease because both qualitative and quantitative judgments are more straightforward in idealized geometries. On the other hand, realistic models have the advantage of capturing various aspects of the modelling problem more vividly, which makes them very useful in a variety of real-life applications (Buist *et al* 2004, Pullan *et al* 2004, Rashev *et al* 2000, 2002).

The simplest of all idealized models describing GEA in the context of the quasistatic approximation to Maxwell's equations is the single-dipole model (Bradshaw *et al* 2001, Hämäläinen and Sarvas 1987, Irimia and Bradshaw 2003). Although it makes use of significant simplifications of the actual phenomenon, this model has proved to be useful not only in GI modelling but also in the study of electrophysiology in other organs, most notably the brain (Gaumond *et al* 1983, Hämäläinen and Sarvas 1987, Hämäläinen *et al* 1993, Mosher *et al* 1992, Sarvas 1987, Wikswo *et al* 1993). In one of our previous studies (Irimia and Bradshaw 2003), it was shown using a simple, two-dipole model that solutions to the inverse problem based on SQUID GI data can allow one to detect abnormal current propagation in humans. Later on, a theoretical ellipsoidal model of the stomach based on the concept of the polarized annular band was used to simulate the electric potential associated with the GEA (Irimia and Bradshaw 2003); this drew attention to the significant modelling advantages offered by the similarities between ellipsoidal geometry and gastric anatomy. We have undertaken the present study with the purpose of creating a GEA forward model in ellipsoidal geometry using current dipoles in the quasistatic approximation.

In the following section, we summarize the theoretical model derived in Kariotou (2004), where analytic expressions for computing the electric potential due to electric dipoles located within an ellipsoid are presented. We then comment on our computational approach and discuss the results of our simulations, particularly in terms of their realism; we conclude that the ellipsoidal model is quite promising in terms of simulating gastric electrical activity. Finally, we comment on the accuracy of the analytical expansions for the potential derived in (Kariotou 2004) and employed in our study.

2. The theoretical model

We adopt the standard equation of the ellipsoid

$$\frac{x_1^2}{\alpha_1^2} + \frac{x_2^2}{\alpha_2^2} + \frac{x_3^2}{\alpha_3^2} = 1, \tag{1}$$

where (x_1, x_2, x_3) are the usual Cartesian coordinates (x, y, z) and

$$0 < \alpha_3 < \alpha_2 < \alpha_1 < +\infty \tag{2}$$

are the ellipsoidal semi-axes. As in Hobson (1955) and Kariotou (2004), we make use of the ellipsoidal system, with coordinates ρ, μ and ν and semifocal distances h_1, h_2 and h_3. Conversion from ellipsoidal to Cartesian coordinates can be made via the relationships

$$x_1 = \frac{\rho\mu\nu}{h_2 h_3} \tag{3}$$

$$x_2 = \frac{\sqrt{\rho^2 - h_3^2}\sqrt{\mu^2 - h_3^2}\sqrt{h_3^2 - \nu^2}}{h_1 h_3} \tag{4}$$

$$x_3 = \frac{\sqrt{\rho^2 - h_2^2}\sqrt{h_2^2 - \mu^2}\sqrt{h_2^2 - \nu^2}}{h_1 h_2}, \tag{5}$$

where $\rho \in [h_2, +\infty)$, $\mu \in [h_3, h_2]$ and $\nu \in [-h_3, h_3]$.

Consider a point $\mathbf{r}_0$ located inside a body of volume V, where a primary current dipole source with moment $\mathbf{Q}$ is also located. The algebraic expression for the current density function (Hämäläinen and Sarvas 1987, Sarvas 1987)

$$\mathbf{J}^p(\mathbf{r}) = \mathbf{Q}\delta(\mathbf{r} - \mathbf{r}_0) \tag{6}$$

allows one to model the phenomenon at hand as a concentration of impressed current $\mathbf{J}^p$ to a point $\mathbf{r}_0$ using the Dirac delta functional $\delta(\mathbf{r} - \mathbf{r}_0)$. The electric field $\mathbf{E}$ induced by the impressed current creates an induction current

$$\mathbf{J}^V(\mathbf{r}) = \sigma\mathbf{E}(\mathbf{r}), \tag{7}$$

where σ is the tissue conductivity. Since anatomical and physiological characteristics of the human body allow for such currents to be considered quasistatic (Hämäläinen *et al* 1993, Malmivuo and Plonsey 1995, Sarvas 1987, Sommerfeld 1952), the electric field is irrotational and Poisson's equation can be used to find the electric potential u.

The formulae for the electric potential due to dipoles located inside ellipsoids, spheroids and spheres were derived by Kariotou (2004). For this reason, we discuss these theoretical results only to the extent that they are necessary for understanding our study. To calculate the electric potential due to a dipole located within an ellipsoid, separation of variables for

Laplace's equation in ellipsoidal coordinates leads to the Lamé equation, which assumes the form

$$\left(x_i^2 - h_3^2\right)\left(x_i^2 - h_2^2\right)E''(x_i) + x_i\left(2x_i^2 - h_3^2 - h_2^2\right)E'(x_i) + \left[\left(h_2^2 + h_3^2\right)P - n(n+1)x_i^2\right]E(x_i) = 0, \tag{8}$$

where P, n are constants, the prime in E' indicates differentiation with respect to the independent variable $x_i = \rho, \mu$ or ν and the factors E are the so-called Lamé functions that form the interior harmonic function

$$\mathbb{E}_n^m(\rho, \mu, \nu) = E_n^m(\rho)E_n^m(\mu)E_n^m(\nu). \tag{9}$$

Among other scientific areas, the mathematical theory of ellipsoidal harmonics is also of interest in gravitational astrophysics (Romain and Barriot 2001), physical geodesy (Featherstone and Dentith 1997) and numerical analysis, e.g., for obtaining solutions to the ellipsoidal Stokes problem (Ritter 1998). The general solution to Poisson's equation

$$\Delta u^-(\mathbf{r}) = \frac{1}{\sigma}\nabla\cdot\mathbf{J}^p(\mathbf{r}), \qquad \mathbf{r}\in V^- \tag{10}$$

in this coordinate formulation is a superposition of an interior harmonic function $\Phi(\mathbf{r})$ and of the function

$$V(\mathbf{r}) = \frac{1}{4\pi\sigma}\mathbf{Q}\cdot\nabla\frac{1}{|\mathbf{r}-\mathbf{r}_0|}, \tag{11}$$

where the superscripts $(-)$ and $(+)$ denote quantities referring to the interior and exterior, respectively, of the volume for which Poisson's equation is solved (in this case the volume V is the ellipsoid). Upon substitution of the formulae for the interior harmonic function and Laplace operator (Miloh 1973) into equation (10), the interior potential assumes the form

$$u^-(\mathbf{r}) = \sum_{n=0}^{\infty}\sum_{m=1}^{2n+1}\left\{b_n^m + \frac{1}{\sigma\gamma_n^m}\left[\mathbf{Q}\cdot\nabla_{\mathbf{r}_0}\mathbb{E}_n^m(\mathbf{r}_0)\right]I_n^m(\rho)\right\}\mathbb{E}_n^m(\rho,\mu,\nu). \tag{12}$$

In the equation above, I_n^m are elliptic integrals of the form

$$I_n^m(\rho) = \int_\rho^\infty \frac{\mathrm{d}t}{\left[E_n^m(t)\right]^2\sqrt{t^2-h_2^2}\sqrt{t^2-h_3^2}} \tag{13}$$

with $n = 0, 1, \ldots, m = 1, 2, \ldots, 2n+1$. Throughout this section, we also use the symbols b_n^m, γ_n^m, Λ and Λ'. b_0^1 is an arbitrary constant whose presence ensures that the potential is invariant under gauge transformations (we assign to it the value 0 in this study), while the rest are normalization constants whose formulae are given in equations (27)–(32) and (44) of Kariotou (2004) in terms of the α_i and spatial coordinates x_i.

As one can see, the interior potential is an infinite summation of terms involving the ellipsoidal harmonics $\mathbb{E}_n^m$. According to a result by Stieltjes (Ritter 1995, Ritter 1997), the Lamé function $E_n^m(\rho)$ (equation (13) in Ritter (1995)) has at most n simple zeros $\theta_{n,m}^1, \ldots, \theta_{n,m}^k, k \leqslant n$. Because identifying all roots is algebraically impossible for polynomials of order 5 and higher, analytic expressions for u exist only up to second order in $\mathbb{E}_n^m$. Better approximations to the electric potential could, in principle, be obtained only by implementing a numerical algorithm for finding roots or with another numerical technique. Alternatively, it may be possible to follow the approach of Hobson (1955) and to derive the required higher order contributors to u by making use of certain relationships between ellipsoidal and spherical harmonics (see Dechambre and Scheeres (2002) and Ritter (1998) for a detailed review of this theoretical problem). In this study, we adopt the approach of

Kariotou (2004) and compute the potential using only terms that involve polynomials of degree less than 3. The potential thus obtained is given by

$$
\begin{aligned}
u^{-}(\mathbf{r}) \approx b_0^1 &+ \frac{3}{4\pi\sigma}\sum_{m=1}^{3} Q_m x_m \left[I_1^m(\rho) - I_1^m(\alpha_1) + \frac{1}{\alpha_1\alpha_2\alpha_3} \right] \\
&- \frac{5}{4\pi\sigma\,(\Lambda-\Lambda')}\sum_{m=1}^{3} Q_m x_{0m} \left[I_2^1(\rho) - I_2^1(\alpha_1) + \frac{1}{2\alpha_1\alpha_2\alpha_3\Lambda} \right] \frac{\mathbb{E}_2^1(\mathbf{r})}{\Lambda-\alpha_m^2} \\
&+ \frac{5}{4\pi\sigma\,(\Lambda-\Lambda')}\sum_{m=1}^{3} Q_m x_{0m} \left[I_2^2(\rho) - I_2^2(\alpha_1) + \frac{1}{2\alpha_1\alpha_2\alpha_3\Lambda'} \right] \frac{\mathbb{E}_2^2(\mathbf{r})}{\Lambda'-\alpha_m^2} \\
&+ \frac{15}{4\pi\sigma}\sum_{\substack{i,j=1\\ i\neq j}}^{3} Q_i x_{0j} x_i x_j \left[I_2^{i+j}(\rho) - I_2^{i+j}(\alpha_1) + \frac{1}{\alpha_1\alpha_2\alpha_3\left(\alpha_i^2+\alpha_j^2\right)} \right]. \qquad (14)
\end{aligned}
$$

Analogously, the formula for the exterior potential u^{+} is given by

$$
\begin{aligned}
u^{+} \approx b_0^1 \frac{I_0^1(\rho)}{I_0^1(\alpha_1)} &+ \frac{3}{4\pi\sigma\alpha_1\alpha_2\alpha_3}\sum_{m=1}^{3} Q_m x_m \frac{I_1^m(\rho)}{I_1^m(\alpha_1)} - \frac{5}{8\pi\sigma\alpha_1\alpha_2\alpha_3(\Lambda-\Lambda')} \\
&\times \sum_{m=1}^{3} Q_m x_{0m} \left[\frac{I_2^1(\rho)}{I_2^1(\alpha_1)} \frac{\mathbb{E}_2^1(\mathbf{r})}{\Lambda\left(\Lambda-\alpha_m^2\right)} - \frac{I_2^2(\rho)}{I_2^2(\alpha_1)} \frac{\mathbb{E}_2^2(\mathbf{r})}{\Lambda'\left(\Lambda'-\alpha_m^2\right)} \right] \\
&+ \frac{15}{4\pi\sigma\alpha_1\alpha_2\alpha_3}\sum_{\substack{i,j=1\\ i\neq j}}^{3} \frac{Q_i x_{0j} x_i x_j}{\alpha_i^2+\alpha_j^2} \frac{I_2^{i+j}(\rho)}{I_2^{i+j}(\alpha_1)}. \qquad (15)
\end{aligned}
$$

As already noted, the formulae above involve only ellipsoidal harmonic terms of degree 1 and 2; this effectively constitutes an approximation of the expression in equation (12), which is an infinite summation of such terms. More on the possible effect of this approximation will be said in a future section.

3. The computational approach

We adopt a gain transfer matrix approach (Mosher 1993) to compute the electric potential due to dipoles located inside an ellipsoid. In this formulation, the vector $\mathbf{v}$ containing computed electric potential values at time j can be modelled as

$$
\begin{aligned}
\mathbf{v}(j) &= \sum_{i=1}^{p} \mathbf{G}(\mathbf{l}_i)\mathbf{q}_i(j) \\
&= [\mathbf{G}(\mathbf{l}_i)\cdots\mathbf{G}(\mathbf{l}_p)][\mathbf{q}_1(j)\cdots\mathbf{q}_p(j)]^T \\
&= \mathbf{G}(\mathbf{l})\mathbf{q}(j), \qquad (16)
\end{aligned}
$$

where the superscript T indicates the transpose of a matrix and

$$\mathbf{l} = [\vec{\mathbf{l}}_1\cdots\vec{\mathbf{l}}_p]^T \qquad (17)$$

$$\mathbf{q} = [\vec{\mathbf{q}}_1\cdots\vec{\mathbf{q}}_p]^T \qquad (18)$$

are column vectors that consist of concatenations of parameters for the p dipoles. The quantities $\vec{\mathbf{l}}_i$ and $\vec{\mathbf{q}}_i$ are 3-vectors indicating the locations and orientations of the dipoles, respectively. The matrix $\mathbf{G}$ is called the 'gain transfer matrix' for the ith dipole. If the dipole

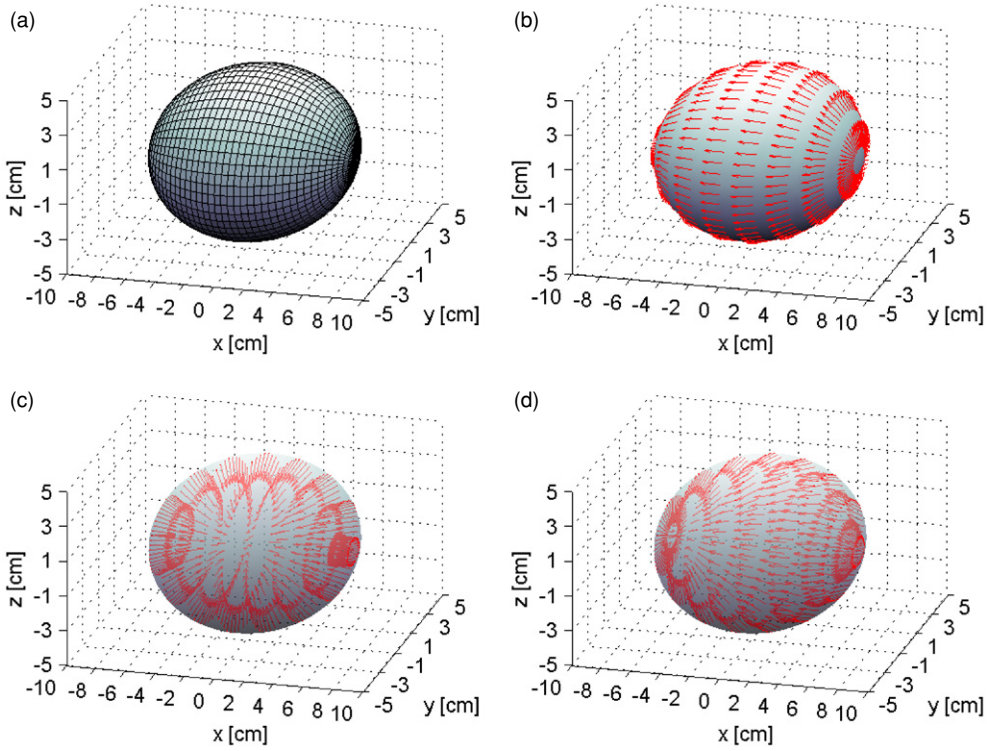

Figure 1. Geometric models for the forward problem of electrogastrography. In these figures, the stomach is simulated as an ellipsoid with $(\alpha_1, \alpha_2, \alpha_3) = (7.5, 5.0, 4.0)$ cm. Propagation starts on the right-hand side, from the extremity of the ellipsoid, and proceeds along the x-axis in the negative x direction. In (a), only the mesh definition is shown. In (b), the propagation surface is shown with dipoles oriented in the direction of propagation. Each circular band of dipoles corresponds to a particular time point during the propagation cycle. For illustration purposes, dipoles are shown only for eight such equidistant time points. In (c), the dipoles are perpendicular to the propagation surface and in (d) the dipole vectors have a component that is parallel to the direction of propagation and another that is perpendicular to it. The body of the ellipsoid in (a) and (b) is opaque, whereas in (c) and (d) it is transparent so as to allow one to visualize the dipole vectors located inside the ellipsoid.

locations are kept constant while their orientations are varied with time, the model can be extended to capture the time-dependent variability of the sources. Thus, for n time points, we have

$$\begin{aligned}\mathbf{A} &= [\mathbf{a}_1 \cdots \mathbf{a}_n] \\ &= \mathbf{G}(\mathbf{l})[\mathbf{q}_1 \cdots \mathbf{q}_n] \\ &= \mathbf{G}(\mathbf{l})\mathbf{Q}. \end{aligned} \tag{19}$$

In our problem, the entries in the gain transfer matrix are computed using the formulae for the potential presented in the previous section to obtain the potential due to each dipole at the required locations.

The geometry of our problem is shown in figure 1. Each propagation cycle begins on the right-hand extremity of the ellipsoid (positive x) and the direction of propagation is the negative x direction. As shown in the figure, the paths assumed by the dipoles are directed longitudinally, along the greater dimension of the idealized gastric body. Each incremental

time step during the propagation process brings about a change in the position of the activation front along the axis of propagation, as the image suggests. Distance increments in the activation front position along the propagation path are equal for all time segments. In other words, the longitudinal lines drawn from the positive to the negative extremity of the ellipsoid in the x direction correspond to the paths assumed by the current dipoles during propagation. The elliptic 'slices' whose lines are perpendicular to the direction of propagation correspond to the time points of the simulation. In our approach, 20 s are necessary for the simulated activation front to propagate from one end of the ellipsoid to the other.

To compute the appropriate locations of the dipoles during each cycle (based on the restriction that the distances between consecutive time points must be equal), the line (path) integral of each current dipole is computed along the direction of propagation, over the extent of each time segment involved. Since the path is a semi-ellipse as indicated by the geometry, the resulting expression assumes the form

$$\begin{aligned}\int_{t_1}^{t_2} \mathrm{d}s &= \int_{t_1}^{t_2} \sqrt{1+\left(\frac{\partial y}{\partial x}\right)^2}\,\mathrm{d}x \\ &= \int_{t_1}^{t_2} \sqrt{1+\frac{\alpha_2^2 x^2}{\alpha_1^4}\left(1-\frac{x^2}{\alpha_1^2}\right)^{-1}}\,\mathrm{d}x, \end{aligned} \tag{20}$$

where ds is the path increment and $t_{1,2}$ are any two successive time points during the propagation cycle. In our computational approach, the integral above is computed numerically using Simpson's $\frac{1}{3}$ rule. This is also done for the elliptic integral in equation (13), which is evaluated numerically. The values assumed for the ellipsoidal semi-axes are $(\alpha_1, \alpha_2, \alpha_3) = (7.5,\ 5.0,\ 4.0)$ cm and an experimentally measured value of 0.45 Ω^{-1} m^{-1} (Bradshaw *et al* 2001) is used for the conductivity σ of the gastric body.

Because the velocity of propagation along the gastric corpus varies from around 0.3 mm s^{-1} at the beginning of a cycle to approximately 4–5 mm s^{-1} at the end (Mirizzi and Scafoglieri 1983), this characteristic was also included into our model. Specifically, a linear dependence of the propagation velocity upon time was assumed for the purpose of our study and the initial and final velocities mentioned above were used to determine the appropriate velocity function. Because our dipoles travel along an ellipsoid and their trajectories are therefore semi-elliptical, the distances travelled by the dipoles were used to associate their locations during the simulation with corresponding time points during the propagation cycle. This was necessary because, although the distance increments used were the same due to our mesh definition (see figure 1), the nature of the velocity function implies that the associated time increments are not. In computing the appropriate time intervals corresponding to equidistant points of successive displacement along the dipole trajectory, the elliptic perimeter p was calculated using the rapidly converging Gauss–Kummer series expansion, given by

$$\begin{aligned} p &= \pi(\alpha_1+\alpha_2)\sum_{n=0}^{\infty}\binom{\frac{1}{2}}{n}^2 \zeta^n \\ &= \pi(\alpha_1+\alpha_2)\left(1+\frac{\zeta}{4}+\frac{\zeta^2}{64}+\frac{\zeta^3}{256}+\cdots\right), \end{aligned} \tag{21}$$

where

$$\zeta \equiv \left(\frac{\alpha_1-\alpha_2}{\alpha_1+\alpha_2}\right)^2. \tag{22}$$

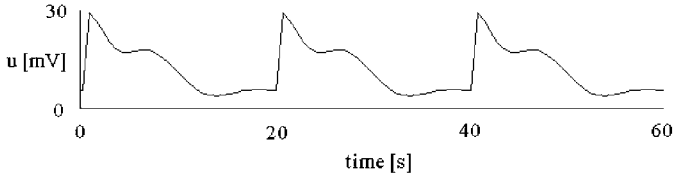

Figure 2. The electric potential u simulated using the ellipsoidal model for a point located on the upper side of the ellipsoidal surface. The orientation of the dipoles used to produce this wave is parallel to the direction of propagation.

An interesting aspect of our problem concerns the orientation of current dipoles during the propagation cycle. In one view concerning this problem, dipoles are oriented inwards with respect to the surface of the ellipsoid, i.e., perpendicular to the surface of propagation. The motivation for this approach is the fact that the cellular exchange of ions in the stomach, mediated by the cells of Cajal, takes place between the concentric tissue layers of the stomach, hence the orientation of the dipoles should be inwards with respect to the propagation surface. The theoretical model capturing this view of the phenomenon was derived by Irimia and Bradshaw in a previous study (Irimia and Bradshaw 2003), to which we refer the reader for the complete derivation. The expression predicting the orientation of current dipoles in this model is given by

$$-q_0 \frac{\nabla \xi}{|\nabla \xi|}, \tag{23}$$

where q_0 is in this case the assumed dipole strength $q_0 = |\mathbf{q}_0|$, $\nabla\xi/|\nabla\xi|$ is the normalized downward unit vector with respect to the ellipsoidal surface S, and ξ is a function whose gradient is perpendicular to S, such that equation (23) is satisfied:

$$\xi(x_1, x_2, x_3) = x_2 - \alpha_2 \sqrt{1 - \frac{x_3^2}{\alpha_3^2} - \frac{x_1^2}{\alpha_1^2}}. \tag{24}$$

The second approach to this problem is based on the fact that propagation is observed in the stomach along the corpus and towards the pylorus and dipoles should therefore be oriented in the direction of propagation. This argument requires the computation of the unit tangent with respect to S, with a direction indicated by the direction of propagation along the surface.

To help clarify this issue, we have chosen to produce simulations using both models, in order to determine which one captures the characteristics of the GEA more suitably. In the first case, the dipole orientation function is computed analytically; in the second case, advantage is taken of the geometry and mesh definition shown in figure 1 to compute the unit tangent vector numerically, using a simple interpolation algorithm. Finally, a third type of simulation was generated, in which the dipole orientation function is a linear combination with different weights of the two functions described above.

4. Results and discussion

Computational results of our simulations are presented in figures 2 and 3. The point for which the potential is evaluated corresponds, in both cases, to the extremity of the ellipsoid in the z (vertical) direction. Thus our waveforms attempt to reproduce the bioelectric potential as recorded on the upper extremity of the gastric wall. This simulated waveform agrees reasonably well with experiment and with other simulations obtained with various models

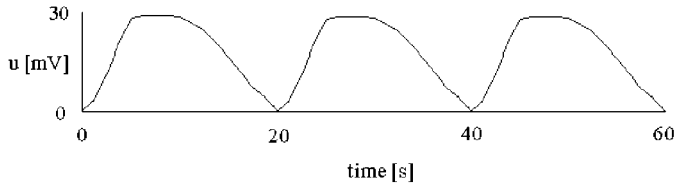

Figure 3. Same as figure 2, but the orientation of the dipoles is perpendicular (as opposed to parallel) to the direction of propagation.

(see, for example, Bradshaw *et al* (2001)). Notable features are the presence of the upstroke followed by the sustained repolarization phase, two characteristics that have been observed experimentally and explained theoretically by activation models (Bradshaw *et al* 2001, Irimia and Bradshaw 2004). In figure 2, the orientation of the dipoles is along the direction of propagation, as opposed to figure 3, where the dipoles are perpendicular to the ellipsoidal surface. The parallel dipole model waveform in figure 2 is able to reproduce the upstroke that is characteristic of experimentally recorded EGG, whereas the perpendicular dipole model in figure 3 is not. In addition to the two cases above, simulations were produced for the scenario where the dipoles had both a parallel ($\mathbf{Q}_p$) and a perpendicular ($\mathbf{Q}_r$) component with respect to the surface of propagation[1] as in figure 1(d), where the linear combination is given by

$$\mathbf{Q} = 0.8\mathbf{Q}_p + 0.2\mathbf{Q}_r. \tag{25}$$

The criterion for the choice of coefficients specified above was based on the physiology and anatomy of the problem. Thus, because the stomach wall is much thinner than it is long with respect to the propagation direction, the coefficient of the perpendicular dipole vector component was selected to be 0.2, i.e., smaller than that for the parallel vector component, which was assigned the value 0.8. With this chosen linear combination of vectors, the resulting waveform was found to be very similar to that in figure 2; this is why, for brevity, it is not reproduced here.

Three-dimensional visualizations of the simulated gastric surface potential are shown in figure 4, where the observed characteristics of the gastric electrical activity are simulated. To acquire a correct understanding of what is conveyed in this figure, it is necessary to analyse it by making close reference to figure 2 because figure 4 shows the evolution of the ellipsoidal surface potential as a function of time for the parallel dipole model. Since the waveform simulated for this model is presented in figure 2, a close relationship exists between the physical quantities depicted in these two figures. Each image in figures 4(a)–(f) depicts a snapshot of the ellipsoidal surface potential throughout the 20 s propagation cycle. In each of these 3D plots, current dipoles are shown in red on the propagation surface with orientations specified by the direction of propagation. The dipoles are located on the isopotential ring where the electric potential reaches a maximum (bright yellow in the figures); this ring corresponds to the potential spike in figure 2. In figures 4(a)–(f), one can also see an elliptic isopotential region immediately behind the ring of propagating dipoles. This band separates the dipole ring (which is at a maximum of the potential) from the portion of the ellipsoid located immediately after the band (where the potential decreases gradually from bright yellow to dark green). The portion of the separating band closest to the ring of dipoles corresponds to the resting potential

[1] The realism of this particular approach and its excellent agreement with noninvasive magnetoenterographic recordings were recently confirmed (July 2005) using the application of an inverse FEM algorithm in the context of a realistic anatomic human model (A S H Lin 2005 Modelling of the slow wave in the small intestine and its associated magnetic field *M. Eng. Thesis* University of Auckland, Auckland, New Zealand).

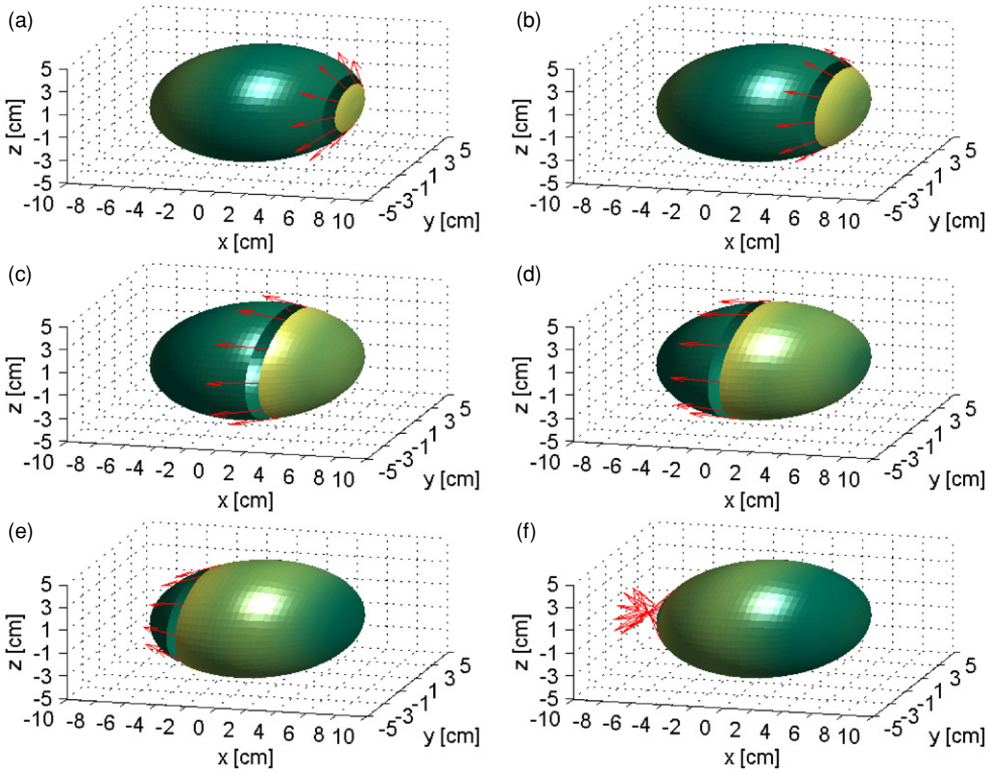

Figure 4. Visualizations of the simulated electric potential on the surface of the ellipsoid throughout an ECA cycle of 20 s. The colour map varies from bright yellow at 30 mV to dark green at 0 mV. The time instants during the propagation cycle that correspond to each of the images in (a)–(f) are (left to right and top down) 3, 7, 10, 13, 17 and 20 s, respectively. In (a), the beginning of a propagation cycle is shown with the associated current dipoles drawn in red with orientations determined by the direction of propagation. The gastric pacemaker is located in this figure on the right-hand extremity of the ellipsoid, in agreement with the physiological characteristics of the stomach. In (b)–(e), the band of dipoles advances along the gastric syncytium in the direction of the pylorus. In (f), the dipoles have reached the pylorus and can be seen as a concentration of red vector arrows on the left-hand extremity of the ellipsoid. On the opposite (right-hand) extremity, a new propagation cycle is about to begin.

plateau depicted in figure 2. Finally, the region of zero potential lying in front of the dipoles on the left-hand side corresponds to the resting potential of the GI tissues after the passage of a dipole band in the previous cycle.

The ellipsoidal model is important at a theoretical level because it offers one of the very few geometries in which expressions for the electric potential and magnetic field due to current dipoles can be formulated analytically. This key aspect of theoretical GI modelling was emphasized in Irimia (2005) and Irimia and Bradshaw (2003), where the ellipsoidal model was used to simulate the gastric electric potential throughout a typical GEA propagation cycle. To further our understanding of the GEA phenomenon, however, it is imperative to improve our knowledge—both qualitative and quantitative—concerning the spatial resolutions of different inverse methods in the context of EGG and MGG. This is important because, although we are now able to detect disease states of the gut, our understanding of pathological GEA remains limited; improved spatial resolution for inverse methods is thus critical for the study of GI

processes at the tissue and even cellular level. In this context, the forward model presented in this paper is relevant in view of future work in the area of inverse algorithm comparison and validation.

To predict the possible diagnostic relevance of our model in the context of inverse modelling, it may be useful to consider the past use of ellipsoidal geometry in the area of fetal MEG (fMEG), where Gutiérrez *et al* (2005) employed an ellipsoidal head model to obtain both forward and inverse solutions that can characterize neural development in newborns. Their motivation for using the ellipsoidal model came from an earlier analysis by Vrba *et al* (2004), who had concluded that the spherical head model was superior to the uniform abdomen model in fMEG. However, because the sphere does not provide an accurate approximation to fetal head anatomy, the ellipsoid was chosen instead by the authors in order to increase the realism of their implementation as well as the ability of their model to capture important fMEG information. Thus, theirs is yet another example showing that the tendency to replace a simple idealized model with one that is more realistic is a powerful driving force in biophysical modelling. A line of reasoning analogous to that of Gutiérrez *et al* quite possibly applies to the case of EGG, where the stomach has been modelled as a cylinder, cone or conoid (Bradshaw *et al* 2001, Mirizzi and Scafoglieri 1983, Rashev *et al* 2000, 2002). Such studies found that idealized models with closer and closer resemblance to gastric anatomy could offer greater and greater improvements in their ability to characterize normal and pathological conditions in humans (Rashev *et al* 2002). Thus, although specific details regarding the superiority of the ellipsoidal EGG inverse model over other candidates are not currently available because inverse solutions have not yet been implemented for it, we believe that the ellipsoidal EGG model may nevertheless be very valuable in light of the arguments presented above. For example, we believe that the uncoupling of gastric electrical sources due to gastroparesis will be easier to characterize with our model than with a simpler, free-space dipole model, which has already been applied to human data with partial success (Irimia and Bradshaw 2004).

To ensure the correctness, accuracy and complete agreement of our computational codes with the theory presented in the previous sections, all calculations were verified by hand for selected values of the electric potential. Because the theoretical model employed here makes use of a truncated infinite summation of ellipsoidal harmonic terms, we have sought to understand the effect of truncation upon the accuracy of the results obtained. In analogy with the theory of spherical harmonics as applied to Laplace's equation, one can expect that the contributions of harmonic terms to the potential should diminish as the order of these terms increases. For the case of a dipole in a sphere, this conclusion can be easily verified by inspection of the formulae for the potential that were first derived by Frank in 1952 (Frank 1952) and later implemented, among others, by Purcell *et al* (1991), Schmidt and Pilkington (1991), and He and Norgren (2000). For the sphere, the expressions for the potential involve, in a manner analogous to the ellipsoidal case, an infinite summation over spherical harmonic terms. However, these expressions have closed forms associated with them (Frank 1952), which eliminates the need for truncating the infinite summations over spherical harmonics when the potential is evaluated. Furthermore, since closed form solutions are available, one does not have to worry about the issue of accuracy that must be taken into account when a truncated expansion is used. In the ellipsoidal case, closed form solutions are not available in the literature. This is a serious drawback because one is then forced to investigate the error associated with the ellipsoidal expansion used to compute the potential. For the problem at hand, expressions for the potential u involving higher order harmonics (degree >3) have not yet been derived (April 2005). As a result, we have attempted to address the issue of accuracy by investigating the extent to which first- and second-order terms contribute to u in our simulations. Because these harmonic terms can be of either negative or positive sign,

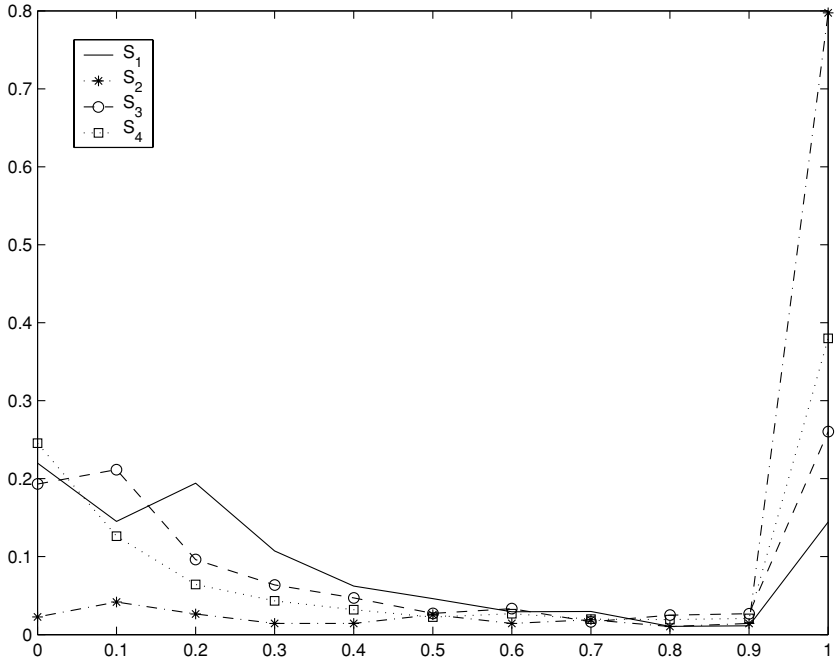

Figure 5. Probability density functions for the magnitudes of ellipsoidal harmonic terms contributing to the potential u computed for the surface of the simulation ellipsoid. The terms $S_i, i = 1, \ldots, 4$ are the four summations (terms of order lower than 3) in equation (14). Although lowest order terms are important, the magnitudes of second-order terms are also non-negligible.

acquiring a quantitative understanding of how much higher versus lower order terms contribute to the actual potential is a delicate matter due to the possible effect of cancellation between terms of identical or different order in equation (14).

In light of these issues, we have chosen to compare the magnitudes of harmonic terms that contribute to each individual value of u computed during a typical simulation. The results of this quantitative comparison is presented in figure 5. To produce this figure, we first normalized the magnitude of every harmonic term contributing to each value of u with respect to that contributor which had the highest magnitude. To explain this in mathematical notation, consider a computed potential value, call it u_1, given numerically by the four terms in equation (14), i.e.,

$$u_1 = b_0 + S_1 - S_2 + S_3 + S_4, \tag{26}$$

where S_1, S_2, S_3 and S_4 are the four summations (terms of order less than 3) in that equation. To compare the contributions of these terms to the potential, the values of $S_i, i = 1, \ldots, 4$ were normalized with respect to $\max\{S_i\}$. During our simulations, the values of these normalized harmonic terms were recorded for all values of the potential evaluated on the surface of the ellipsoid. Furthermore, the probability distribution functions for each of these terms were computed to acquire a quantitative understanding of how important they are to the evaluated potential.

In figure 5, the probability distribution functions of the normalized harmonic terms are presented. As the figure demonstrates, there is a high probability that any of the terms included—regardless of their order—contributes substantially to the computed potential. This becomes apparent upon examination of the probability range [0.9, 1.0] in our figure. Another

issue to be noted is that the significance of contributions by first- and second-order terms to the potential oscillates greatly between the two extremes. What this may imply is that, from a quantitative standpoint, both first- and second-order harmonic terms can be equally important in the evaluation of the potential, at least in the case of the problem at hand. To better understand our argument, it is useful to consider the same potential problem but for the case of the sphere, where the magnitudes of higher degree contributors to the potential decreases rapidly as the degree of such terms increases. If this feature of the spherical problem were to be used to predict the behaviour of high-degree terms in the ellipsoidal case at hand, one would expect that, overall, second-degree terms would contribute less than first-degree terms. This, however, is not what figure 5 suggests. Letting f_k represent the probability density function associated with ellipsoidal terms of order k, figure 5 makes it clear that the terms S_3 and S_4 associated with second-degree terms are important because the integral

$$\int_{0.9}^{1.0} f_k \, \mathrm{d}f \tag{27}$$

for $k = 2$ is comparable in magnitude with the same integral associated with the first-degree terms, for which $k = 1$. In other words,

$$\int_{0.9}^{1.0} f_1 \, \mathrm{d}f \sim \int_{0.9}^{1.0} f_2 \, \mathrm{d}f. \tag{28}$$

This means that, probabilistically, the contributors to the potential associated with the first- and second-degree terms are comparable in magnitude and that the spherical case does not provide a clear analogy with the ellipsoidal case. This may suggest that further theoretical and/or computational investigation is required in order to obtain expressions for u that include harmonic terms of degree higher than 2. Such work may help in clarifying how large the approximation (series truncation) error is for equation (5) as derived in Kariotou (2004). Finally, we note that the importance of high-order ellipsoidal harmonic terms was also emphasized by Sona, who demonstrated that such terms have a significant role when solving geodetic boundary value problems (Sona 1995).

In our modelling case, higher order harmonic terms may not significantly affect the simulated waveforms presented in this paper from a qualitative standpoint. We believe this is the case because of the good qualitative agreement of our present results with experiment and previous studies that used other models. For example, a free-space dipole model implemented by one of the present authors (LAB, see Bradshaw *et al* (2003)) yielded waveforms very similar to ours; furthermore, both our present results and those in Bradshaw *et al* (2003) are in agreement with earlier theoretical studies by Familoni *et al* (who simulated the propagation of dipoles in cylindrical geometry (Familoni *et al* 1987, 1995)) and even with the earlier study of Sarna *et al*, who employed a coupled oscillator model (Sarna *et al* 1971). Our theoretical results are also in agreement with a wide range of experimental results, ranging from a very early study by Bozler (1945) conducted in 1945 to recent ones (2001)–(2004) by Zhu and Chen (2004), Parkman *et al* (2003) and Horiguchi *et al* (2001), etc. Thus, higher order contributors to the potential may not be essential when only forward modelling is concerned. However, the situation may be quite different in the case of inverse modelling. There, because of the ill-position of the inverse problem, small changes in the measured or simulated potential can cause significant changes in the reconstructed sources. The ellipsoidal expansion derivations of Kariotou were published in 2004 (Kariotou 2004). Already, a very recent study by Gutiérrez *et al* (2005) published in 2005 used the very same geometry and harmonic expansions to second order that were employed in this paper to obtain inverse solutions from fetal magnetoencephalographic recordings. Since their approach was applied in the context of encephalography and involved a different number of dipoles with different

activation patterns being studied, our observations regarding the issue of accuracy may not be directly applicable to their study; it would therefore be premature and ill-advised to criticize the accuracy of their results solely on this basis. However, we believe that our present study is timely and extremely important because our results can draw attention to the fact that the issue of ellipsoidal forward model accuracy is not entirely elucidated and needs further investigation. Solving this matter possibly involves the process of validating the use of inverse procedures in ellipsoidal geometry based on an analysis of the error associated with the number of harmonic terms included in the forward model.

5. Conclusion and future research

Modelling the GEA using the ellipsoidal model is useful because it allows one to explore many important problems related to gastric physiology in a simplified and idealized geometry. Although the approximation errors associated with this formulation remain an open issue, we have shown here that the electric waveform simulated with this model is able to reproduce very well key characteristics of the GEA waveform. Future research will have to determine the optimal size of the ellipsoidal harmonic expansion to be included in the forward model when inverse solutions based on such a model are to be attempted.

Acknowledgments

The authors are grateful to A J Pullan and L K Cheng of the Bioengineering Institute at the University of Auckland for their useful comments and suggestions. Funding was provided for this undertaking by the National Institute of Health, grant no 1RO1 DK 58697 and by the Veterans' Affairs Research Service.

References

Allos S H, Staton D J, Bradshaw L A, Halter S, Wikswo J P Jr and Richards W O 1997 Superconducting quantum interference device magnetometer for diagnosis of ischemia caused by mesenteric venous thrombosis *World J. Surg.* **21** 173–8

Bozler E 1945 The action potentials of the stomach *Am. J. Physiol.* **144** 693–700

Bradshaw L A, Allos S H, Wikswo J P Jr and Richards W O 1997 Correlation and comparison of magnetic and electric detection of small intestinal electrical activity *Am. J. Physiol. Gastrointest. Liver Physiol.* **272** G1159–G1167

Bradshaw L A, Richards W O and Wikswo J P Jr 2001 Volume conductor effects on the spatial resolution of magnetic fields and electric potentials from gastrointestinal electrical activity *Med. Biol. Eng. Comput.* **39** 35–43

Bradshaw L A, Myers A G, Wikswo J P Jr and Richards W O 2003 A spatio-temporal dipole simulation of gastrointestinal magnetic fields *IEEE Trans. Biomed. Eng.* **50** 836–47

Buist M L, Cheng L K, Yassi R, Bradshaw L A, Richards W O and Pullan A J 2004 An anatomical model of the gastric system for producing bioelectric and biomagnetic fields *Physiol. Meas.* **25** 849–61

Dechambre D and Scheeres D J 2002 Transformation of spherical harmonic coefficients to ellipsoidal harmonic coefficients *Astron. Astrophys.* **387** 1114–22

Everhart J E 1994 *Digestive Diseases in the United States: Epidemiology and Impact. US Department of Heath and Human Services, National Institutes of Health, National Institute of Diabetes and Digestive and Kidney Diseases* (Washington, DC: US Government Printing Office)

Familoni B O, Kingma Y J and Bowes K L 1987 Noninvasive assessment of human gastric motor function *IEEE Trans. Biomed. Eng.* **34** 30–6

Familoni B O, Abell T L and Bowes K L 1995 A model of gastric electrical activity in health and disease *IEEE Trans. Biomed. Eng.* **42** 647–57

Featherstone W E and Dentith M C 1997 A geodetic approach to gravity data reduction for geophysics *Comput. Geosci.* **23** 1063–70

Frank E 1952 Electric potential produced by two point current sources in a homogeneous conducting sphere *J. Appl. Phys.* **23** 1225–8

Gaumond R P, Lin J-H and Geselowitz D B 1983 Accuracy of dipole localization with a spherical homogeneous model *IEEE Trans. Biomed. Eng.* **30** 29–34

Gutiérrez D, Nehorai A and Preissl H 2005 Ellipsoidal head model for fetal magnetoencephalography: forward and inverse solutions *Phys. Med. Biol.* **50** 2141–57

Hämäläinen M S and Sarvas J 1987 Feasibility of the homogeneous head model in the interpretation of neuromagnetic fields *Phys. Med. Biol.* **32** 91–7

Hämäläinen M S, Hari R, Ilmoniemi R J, Knuutila J and Lounasmaa O 1993 Magnetoencephalography-theory, instrumentation, and applications to noninvasive studies of the working human brain *Rev. Mod. Phys.* **65** 413–97

He S and Norgren M 2000 Magnetostatic image current and its application to an analytic identification of a current dipole inside a conducting sphere *IEEE Trans. Biomed. Eng.* **47** 183–91

Hobson E W 1955 *The Theory of Spherical and Ellipsoidal Harmonics* (Cambridge: Cambridge University Press)

Horiguchi K, Semple G S A, Sanders K M and Ward S M 2001 Distribution of pacemaker function through the tunica muscularis of the canine gastric antrum *J. Physiol.* **537.1** 237–50

Irimia A and Bradshaw L A 2003 Theoretical ellipsoidal model of gastric electrical control activity propagation *Phys. Rev.* E **68** 051905

Irimia A and Bradshaw L A 2004 Theoretical and computational methods for the noninvasive detection of gastric electrical source coupling *Phys. Rev.* E **69** 051920

Irimia A 2005 Electric field and potential calculation for a bioelectric current dipole in an ellipsoid *J. Phys. A: Math. Gen.* **38** 8123–38

Jenks W G, Sadeghi S S H and Wikswo J P Jr 1997 SQUIDS for nondestructive evaluation *J. Phys. D: Appl. Phys.* **30** 293–323

Jiménez M, Borderies J R, Vergara P, Wang Y F and Daniel E E 1999 Slow waves in circular muscle of porcine ileum: structural and electrophysiological studies *Am. J. Phisiol. Gastrointest. Liver Physiol.* **39** G393–G406

Kariotou F 2004 Electroencephalography in ellipsoidal geometry *J. Math. Anal. Appl.* **290** 324–42

Lin X, Hayes J, Peters L J and Chen J D Z 2000 Entrainment of intestinal slow waves with electrical stimulation using intraluminal electrodes *Ann. Biomed. Eng.* **28** 582–7

Malmivuo J and Plonsey R 1995 *Bioelectromagnetism* (New York: Oxford University Press)

Mintchev M P, Otto S J and Bowes K L 1997 Electrogastrography can recognize gastric electrical uncoupling in dogs *Gastroenterol* **112** 2006–11

Mirizzi N and Scafoglieri U 1983 Optimal direction of the elegrogastrographic signal in man *Med. Biol. Eng. Comput.* **21** 385–9

Mosher J C, Leahy R M and Lewis P S 1992 Multiple dipole modeling and localization from spatiotemporal MEG data *IEEE Trans. Biomed. Eng.* **42** 541–57

Mosher J C 1993 Localization from near-source quasi-static electromagnetic fields *PhD Thesis* University of Southern California, pp 16–9

Miloh T 1973 Forces and moments on a triaxial ellipsoid in potential flow *Isr. J. Technol.* **11** 63–74

Nelsen T S and Becker J C 1968 Simulation of the electrical and mechanical gradient of the small intestine *Am. J. Physiol.* **214** 749–57

Parkman H P, Hasler W L, Barnett J L and Eaker E Y 2003 Electrogastrography: a document prepared by the gastric section of the american motility society clinical GI motility testing task force *Neurogastroenterol. Motil.* **15** 89–102

Publicover N G and Sanders K M 1989 Are relaxation oscillators an appropriate model of the gastrointestinal electrical activity? *Am. J. Physiol.* **256** G265–G274

Pullan A, Cheng L, Yassi R and Buist M 2004 Modeling gastrointestinal bioelectric activity *Prog. Biophys. Mol. Biol.* **85** 523–50

Purcell C, Mashiko T, Okada K and Ueno K 1991 Describing head shape with surface harmonic expansions *IEEE Trans. Biomed. Eng.* **38** 303–6

Rashev P Z, Mintchev M P and Bowes K L 2000 Application of an object-oriented programming paradigm in three-dimensional computer modeling of mechanically active gastrointestinal tissues *IEEE Trans. Inf. Technol. Biomed.* **4** 247–58

Rashev P Z, Bowes K L and Mintchev M P 2002 Three-dimensional object-oriented modeling of the stomach for the purpose of microprocessor-controlled functional stimulation *IEEE Trans. Inf. Technol. Biomed.* **6** 296–309

Ritter S 1995 A sum-property of the eigenvalues of the electrostatic integral operator *J. Math. Anal. Appl.* **196** 120–34

Ritter S 1997 On the magnetostatic integral operator for ellipsoids *J. Math. Anal. Appl.* **207** 12–28

Ritter S 1998 The nullfield method for the ellipsoidal Stokes problem *J. Geod.* **72** 101–6

Ritter S 1998 On the computation of Lamé functions, of eigenvalues and eigenfunctions of some potential operators *Z. Angew. Math. Mech.* **78** 66–72

Romain G and Barriot J P 2001 Ellipsoidal harmonic expansions of the gravitational potential: theory and application *Celest. Mech. Dyn. Astron.* **79** 235–75

Rothstein R D, Alavi A and Reynolds J C 1993 Electrogastrography in patients with gastroparesis and effect of long-term cisapride *Dig. Dis. Sci.* **35** 1518–24

Sanders K M 1996 A case for interstitial cells of Cajal as pacemakers and mediators of neurotransmission in the gastrointestinal tract *Gastroenterol* **111** 492–515

Sarna S K, Daniel E E and Kingma Y J 1971 Simulation of slow-wave electrical activity of small intestine *Am. J. Physiol.* **221** 166–75

Sarvas J 1987 Basic mathematical and electromagnetic concepts of the biomagnetic inverse problem *Phys. Med. Biol.* **32** 11–22

Schmidt J A and Pilkington T C 1991 The volume conductor effects of anisotropic muscle on body surface potentials using an eccentric spheres model *IEEE Trans. Biomed. Eng.* **38** 300–3

Serio R, Barajas-Lopez C, Daniel E E, Berezin I and Huizinga J D 1991 Slow-wave activity in colon: role of network of submucosal interstitial cells of Cajal *Am. J. Physiol.* **260** G636–G645

Sharkawi T Y, Morgan K G and Szurszewski J H 1978 Intracellular electrical activity of canine and human gastric smooth muscle *J. Physiol.* **279** 291

Sommerfeld A 1952 *Electrodynamics* (New York: Academic Press)

Sona G 1995 Numerical problems in the computation of ellipsoidal harmonics *J. Geod.* **70** 117–26

Turnbull G K, Ritcey S P, Stroink G, Brandts B and van Leeuwen P 1999 Spatial and temporal variations in the magnetic fields produced by human gastrointestinal activity *Med. Biol. Eng. Comput.* **37** 549–54

Vrba J, Robinson S E, McCubbin J, Murphy P, Eswaran H, Wilson J D, Preissl H and Lowery C L 2004 Human fetal brain imaging by magnetoencephalography: verification of fetal brain signals by comparison with fetal brain models *Neuroimage* **21** 1009–20

Wikswo J P, Gevins A and Williamson S J 1993 The future of EEG and MEG *Electroencephalogr. Clin. Neurophysiol.* **87** 1–9

Zhu H and Chen J D Z 2004 Gastric distension alters frequency and regularity but not amplitude of the gastric slow wave *Neurogastroenterol. Motil.* **16** 745–52